Atmos. Chem. Phys., 25, 7925–7940, 2025
https://doi.org/10.5194/acp-25-7925-2025

Atmospheric Chemistry and Physics
Open Access

Characterization of reactive oxidized nitrogen in the global upper troposphere using recent and historic commercial and research aircraft campaigns and GEOS-Chem

Nana Wei[1], Eloise A. Marais[1], Gongda Lu[1,a], Robert G. Ryan[1,b], and Bastien Sauvage[2]

[1]Department of Geography, University College London, London, UK
[2]Laboratoire d'Aérologie, Université de Toulouse, CNRS, Université Toulouse III Paul Sabatier, Toulouse, France
[a]now at: the Satellite Application Center for Ecology and Environment, Ministry of Ecology and Environment, Beijing, China
[b]now at: School of Geography, Earth and Atmospheric Science, University of Melbourne, Melbourne, Australia

Correspondence: Nana Wei (nana.wei.21@ucl.ac.uk) and Eloise A. Marais (e.marais@ucl.ac.uk)

Received: 30 October 2024 – Discussion started: 3 December 2024
Revised: 12 May 2025 – Accepted: 13 May 2025 – Published: 25 July 2025

Abstract. Reactive oxidized nitrogen (NO_y) in the upper troposphere (UT) influences global climate, air quality, and tropospheric oxidants, but this understanding is limited by knowledge of the relative contributions of individual NO_y components in this undersampled layer. Here, we use sporadic NASA DC-8 aircraft campaign observations, after screening for plumes and stratospheric influence, to characterize UT NO_y composition and to evaluate current knowledge of UT NO_y as simulated by the GEOS-Chem model. The use of DC-8 data follows confirmation that these intermittent data reproduce NO_y seasonality from routine commercial aircraft observations (2003–2019), supporting the use of DC-8 data to characterize UT NO_y. We find that peroxyacetyl nitrate (PAN) dominates UT NO_y (30 %–64 % of NO_y), followed by nitrogen oxides ($NO_x \equiv NO + NO_2$) (6 %–18 %), peroxynitric acid (HNO_4) (6 %–13 %), and nitric acid (HNO_3) (7 %–11 %). Methyl peroxy nitrate (MPN) makes an outsized contribution to NO_y (14 %–24 %) over the Southeast US relative to the other regions sampled (2 %–7 %). GEOS-Chem, sampled along DC-8 flights, exhibits much weaker seasonality than the DC-8, underestimating summer and spring NO_y and overestimating winter and autumn NO_y. The model consistently overestimates peroxypropionyl nitrate (PPN) by ~ 10–16 pptv or 10 %–90 % and underestimates NO_2 by 6–36 pptv or 31 %–65 %, as the model is missing PPN photolysis. A model underestimate in MPN of at least ~ 50 pptv (13-fold) over the Southeast US results from uncertainties in processes that sustain MPN production as air ages. Our findings highlight that a greater understanding of UT NO_y is critically needed to determine its role in the nitrogen cycle, air pollution, climate, and the abundance of oxidants.

1 Introduction

Reactive oxidized nitrogen (NO_y) in the upper troposphere impacts global climate, surface air quality, and the oxidizing capacity of the whole troposphere (Mickley et al., 1999; Bradshaw et al., 2000; Dahlmann et al., 2011; Worden et al., 2011). NO_y is an important climate driver because tropospheric ozone (O_3) production is limited by the availability of NO_y, particularly in the upper troposphere where the radiative forcing efficiency of O_3 peaks (Dahlmann et al., 2011; Worden et al., 2011; Rap et al., 2015). The influence on tropospheric O_3 production also affects the abundance of the main atmospheric oxidant, the hydroxyl radical (OH), thus altering the lifetimes of the longer-lived greenhouse gas methane and the air pollutants carbon monoxide (CO) and volatile organic compounds (VOCs) (Murray et al., 2013; Seltzer et al., 2015).

Knowledge of dominant daytime NO_y compounds, sources, chemistry, fate, and persistence in the upper troposphere has been largely informed by observations and models used as part of research and commercial aircraft campaigns (Boersma et al., 2011; Marais et al., 2018; Silvern et al., 2018; Travis et al., 2016, 2020). Instruments onboard research aircraft that sample the upper troposphere, in particular the recently retired NASA DC-8 platform, have undergone substantial development to directly measure and derive estimates of a large suite of upper tropospheric NO_y compounds. These include nitrogen oxides ($NO_x \equiv NO + NO_2$), peroxyacetyl nitrate (PAN), and other prominent PAN-type compounds, nitric acid (HNO_3), peroxynitric acid (HNO_4), alkylnitrates (ALKNs) and, more recently, methyl peroxy nitrate (MPN).

These aircraft campaigns have confirmed that sources of NO_y to the upper troposphere are dominated by lightning NO_x emissions (Levy et al., 1999; Gressent et al., 2014, 2016; Marais et al., 2018), causing a seasonal maximum in NO_y in the summer months and a minimum in the winter in parts of the world, such as the northern midlatitudes, where there is large seasonal variability in lightning activity (Blakeslee et al., 2014; Stratmann et al., 2016). Other NO_y source contributors include NO_x emissions from cruising altitude aircraft (Brasseur et al., 1996), stratospheric downwelling of air masses laden with HNO_3 and NO_2 that also promote prompt formation of PANs on mixing with cold upper tropospheric air (Levy et al., 1980; Jacob et al., 2010; Liang et al., 2011), deep convective uplift of surface pollution (Ehhalt et al., 1992; Jaeglé et al., 1998; Bertram et al., 2007), and aged air masses, initially very photochemically active, that accumulate MPN (Nault et al., 2015).

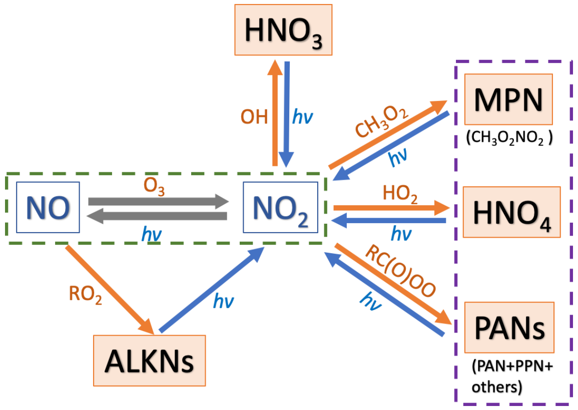

Figure 1. Dominant daytime reactive oxidized gas-phase nitrogen components and reaction pathways in the upper troposphere. Arrow colours distinguish formation (orange) and photolytic ($h\nu$) decomposition (blue) of reservoir compounds. Dashed boxes indicate compounds of the NO_x family (green) and those classed as peroxy nitrates (purple). "R" in RC(O)OO and RO_2 represents an alkyl group.

Chemical cycling of dominant daytime NO_y components, informed by past review and measurement compilation studies of the free troposphere (Emmons et al., 1997; Bradshaw et al., 2000), is illustrated in Fig. 1. During the day, NO and NO_2 are in a photostationary steady state, as NO oxidation, mostly by O_3, is balanced by NO_2 photolysis. NO_x also reacts to form reservoir compounds. For NO_2, these include HNO_3 from reaction with OH, PANs from reaction with peroxy acyl radicals (RC(O)OO), HNO_4 from reaction with the hydroperoxyl radical (HO_2), and MPN from reaction with the methyl peroxy radical (CH_3O_2). PANs in the upper troposphere are typically dominated by PAN, followed by peroxypropionyl nitrate (PPN) (Singh, 1987; Roberts, 1990; Roberts et al., 1998, 2002). For NO, reservoir compounds include ALKNs from reaction with non-acyl peroxy radicals (RO_2). Recycling of reservoir compounds back to NO_x is dominated by photolysis, as thermally labile peroxy nitrates (PNs) including PANs, HNO_4, and MPN are stable against decomposition in the cold upper troposphere (Huey, 2007). This recycling, along with NO_y sources to the upper troposphere, sustains upper tropospheric NO_x concentrations at ~ 30 pptv over the remote ocean and ~ 100 pptv over polluted landmasses (Marais et al., 2018, 2021; Shah et al., 2023). Stable NO_x reservoir compounds are transported long distances before subsiding and decomposing on warming, thus supplying other parts of the world with oxidants (HO_x) and O_3 precursors (NO_x and peroxy radicals) (Schultz et al., 1999). Loss processes in the dry upper troposphere are slow and dominated by subsidence, resulting in long NO_y lifetimes of 10–20 d (Logan, 1983; Prather and Jacob, 1997). Similarly, NO_x has a lifetime of about a week compared to less than a day in the boundary layer (< 2 km) (Jaeglé et al., 1998).

Nighttime NO_y chemistry is also important, but aircraft campaign measurements of the nocturnal upper troposphere mostly consist of total NO_y from commercial aircraft campaigns. The nighttime chemistry not shown in Fig. 1 includes NO reaction with OH, forming nitrous acid (HONO) that accumulates in the absence of photolysis as well as NO_2 reaction with O_3 to form the nitrate radical (NO_3), which further reacts with NO_2 to produce N_2O_5, a precursor of aerosol nitrate (pNO_3) (Bradshaw et al., 2000).

Modelling studies evaluating the best understanding of NO_y in the upper troposphere routinely identify stark discrepancies between observed and modelled total NO_y, NO_x, and the ratio of NO-to-NO_2 in the upper layers of the troposphere (Jaeglé et al., 1998; Talbot et al., 1999; Bertram et al., 2007; Hudman et al., 2007; Liang et al., 2011; Nault et al., 2015; Huntrieser et al., 2016; Travis et al., 2016; Fisher et al., 2018; Silvern et al., 2018; Lee et al., 2022; Cohen et al., 2023). These studies have either focused on a few NO_y components or a single aircraft campaign. A more holistic investigation of all NO_y components is needed, as advocated by Murray et al. (2021), to reduce uncertainties in knowledge of the current, past, and potential future abundances of tropospheric oxidants. Past studies have also documented the challenges of examining measurements made in the upper troposphere. These include screening for stratospheric influence, determining the height of the chemical tropopause, and selecting observations and campaigns that are climatologically representative of a standard atmosphere (Weinheimer et al., 1994; Fuelberg et al., 2000; Bertram et al., 2007; Barth et al., 2015; Huntrieser et al., 2016). Instruments measuring NO_2 are also susceptible to interference from decomposition of the least thermally stable NO_x reservoir compounds, HNO_4 and MPN, that are abundant in the cold upper troposphere (Ryerson et al., 2000; Shah et al., 2023). NO_y from these same instruments can also be biased by decomposition of non-NO_y fixed nitrogen compounds prevalent in the upper troposphere, such as hydrogen cyanide (HCN) (Bradshaw et al., 1998).

Here, we use NASA DC-8 research and In-service Aircraft for a Global Observing System (IAGOS) commercial aircraft campaign measurements, each spanning more than a decade, to characterize global NO_y seasonality and composition in the upper troposphere. This follows careful campaign and data selection to isolate observations sampling the upper troposphere under standard conditions for broad assessment of consistent NO_y seasonality between DC-8 and routine commercial aircraft campaign observations. We go on to use the DC-8 data to critique contemporary understanding of upper tropospheric NO_y as simulated by the GEOS-Chem model.

2 Materials and methods

2.1 Research aircraft observations of total and components of NO_y

The DC-8 research aircraft has sampled ambient air covering the near full extent of the troposphere since its maiden campaign in 1985 (Culter, 2009). Many of the initial campaigns included instruments that measured a subset of the NO_y components shown in Fig. 1, typically continuous measurements of total NO_y, NO, HNO_3, PAN and PPN, and whole air sampler (WAS) collection and laboratory detection of C1–C5 ALKNs (Singh et al., 1999). Since 2004, DC-8 campaigns have included continuous measurements of HNO_4, other PAN-type species, and total PNs (Singh et al., 2006). Given this, we only consider DC-8 campaigns with a relatively consistent suite of instruments that mostly sampled well-mixed air representative of a climatologically standard atmosphere. These criteria eliminate the summer 2004 Intercontinental Chemical Transport Experiment-North America (INTEX-NA) campaign (Singh et al., 2006; Singh et al., 2009), which is the only DC-8 campaign since 2004 not to include a NO_x and NO_y chemiluminescence analyser, and the summer 2012 Deep Convective Clouds and Chemistry (DC3) campaign, which targeted convective thunderstorms influenced by fresh surface pollution and lightning NO_x emissions (Barth et al., 2015).

The DC-8 campaigns we use are the Arctic Research of the Composition of the Troposphere from Aircraft and Satellites (ARCTAS) over the Arctic and sub-Arctic in spring and summer 2008 (Jacob et al., 2010), the Studies of Emissions and Atmospheric Composition, Clouds and Climate Coupling by Regional Surveys (SEAC^{4}RS) over the Southeast US in late summer and early autumn 2013 (Toon et al., 2016), the Korea-United States Air Quality (KORUS-AQ) over South Korea in late spring and early summer 2016 (Crawford et al., 2021), and the Atmospheric Tomography Mission (ATom), which included four sub-campaigns along the same flight path from pole to pole over the Atlantic and Pacific Oceans in all four seasons from 2016 to 2018 (Thompson et al., 2021). ATom sub-campaigns are ATom-1 in July–August, ATom-2 in January–February, ATom-3 in September–October, and ATom-4 in April–May. The data for these campaigns are from NASA data portals for each campaign, downloaded as merged 1 min files for ARCTAS (NASA, 2009), SEAC^{4}RS (NASA, 2015), and KORUS-AQ (NASA, 2017) and as two separate merged files for ATom, with the WAS C1–C5 ALKNs data at variable time intervals of 40 s, 1, and 2 min and without the WAS C1–C5 ALKNs data at 1 min resolution (NASA, 2021).

Figure 2 shows the global sampling extent of the upper troposphere by NASA DC-8 after applying filtering criteria to the data to isolate observations representative of photochemical steady state (PSS) conditions. For this, we select daytime (08:30–15:30 local solar time or LST) observations within a wide pressure range from 180 hPa ($\sim$ 8 km) to the DC-8 ceiling of 450 hPa ($\sim$ 12 km). This captures the full vertical extent of the midlatitude upper troposphere but not the tropics. The tropical tropopause, according to NASA Modern-Era Retrospective analysis for Research and Applications version 2 (MERRA-2) meteorology, extends to $\sim$ 16 km. We separate the stratosphere from the troposphere with a tropopause definition that can be applied to all datasets. We remove data with observed O_3 concentrations above thresholds that represent the location of the chemical tropopause (Zahn et al., 2002). The thresholds we use are a single year-round value for the tropics (20° N to 20° S) of 100 ppbv (Dameris, 2015) and seasonally varying values everywhere else calculated using the day-of-year dependent O_3 tropopause equation derived by Zahn et al. (2002) from the inverse relationship between O_3 and CO observations from commercial aircraft campaigns. These are 120 ppbv in spring, 103 ppbv in summer, 74 ppbv in autumn, and 91 ppbv in winter. We also screen for stratospheric intrusions (identified as observations with $O_3/CO > 1.25\ \mathrm{mol\,mol^{-1}}$) (Hudman et al., 2007), fresh NO_x emissions ($NO_y/NO < 3\ \mathrm{mol\,mol^{-1}}$), fresh convection (large (> 10 nm diameter) condensation nuclei $> 10^4\ \mathrm{cm^{-3}}$), biomass burning plumes (CO > 200 ppbv and acetonitrile > 200 pptv) (Shah et al., 2023) as well as instances where NO_2 photolysis frequencies are approximately

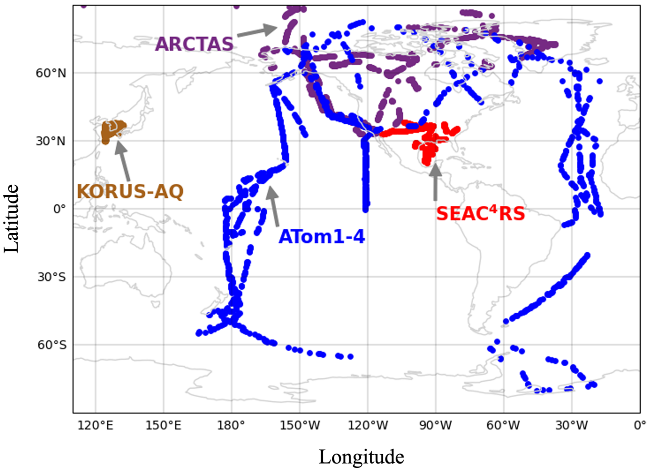

Figure 2. Extent of NASA DC-8 sampling of the upper troposphere under standard, steady state conditions. Colours distinguish ARCTAS (plum), SEAC^{4}RS (red), KORUS-AQ (brown), and ATom (blue). ATom points are 1 min resolution data.

zero. The latter removes high latitude ATom measurements obtained at 08:30–15:30 LST under dark conditions during polar twilight or polar night. The data that are retained correspond to solar zenith angles $\leq 80°$ in polar regions and $\leq 60°$ at other latitudes. The proportion of observations at 450–180 hPa is 42 %–50 % for ATom and 16 %–37 % for the other campaigns. After applying all other data screening, 20 % of all data are retained for ATom and 7 %–11 % for the other campaigns.

The DC-8 instruments measuring NO_y components (Fig. 1) that are common to all campaigns include a chemiluminescence instrument measuring NO, NO_2, and total NO_y (Ryerson et al., 2000; Pollack et al., 2010; Bourgeois et al., 2022), a chemical ionization mass spectrometer (CIMS) measuring HNO_3 (Crounse et al., 2006), a CIMS measuring HNO_4, PAN, PPN, and other PANs (Huey, 2007), and a Whole Air Sampler (WAS) collecting samples analysed in the laboratory using gas chromatography with flame ionization and atomic emission to detect C1–C5 ALKNs (Blake et al., 2003). The other PANs measured with the CIMS include peroxyacryloyl nitrate (APAN), peroxyisobutyryl nitrate (PiBN), peroxybutyryl nitrate (PBN), and peroxybenzoyl nitrate (PBZN). Other instruments deployed for select campaigns are Thermal-Dissociation Laser Induced Fluorescence (TD-LIF) measuring NO_2, total PNs, and total ALKNs (ARCTAS, KORUS-AQ, SEAC^{4}RS) (Day et al., 2002) and the PAN and Trace Hydrohalocarbon ExpeRiment (PANTHER) instrument measuring PAN (ATom). There are also TD-LIF methyl peroxy nitrate (MPN) measurements reported in the SEAC^{4}RS dataset and derived for ARCTAS by Browne et al. (2011).

Concentrations of NO_2 in the upper troposphere are close to chemiluminescence instrument uncertainty (Pollack et al., 2010; Bourgeois et al., 2022), and the measurements include interference from decomposition of NO_x reservoir compounds in the instrument inlet. The Reed et al. (2016b) temperature-dependent inlet temperature decomposition profiles of individual NO_x reservoir compounds for an instrument similar to that operated on the DC-8 suggest interference of 80 %–100 % MPN and 15 %–45 % HNO_4 for the typical inlet temperature range of the DC-8 chemiluminescence instrument of 20–30 °C (Bourgeois et al., 2022). For the campaigns that measured HNO_4 and derived or measured MPN, this amounts to 13–27 pptv for ARCTAS and 71–92 pptv for SEAC^{4}RS. Given this, we instead calculate NO_2 using the NO–NO_2 photochemical steady state (PSS) approximation, as is now standard (Travis et al., 2016; Shah et al., 2023; Horner et al., 2024). Conversion of NO to NO_2, mostly (75 %) due to oxidation by O_3 in the upper troposphere (Silvern et al., 2018), is balanced by NO_2 photolysis back to NO:

$$\mathrm{NO} \xrightarrow{\mathrm{O_3/HO_2/BrO}} \mathrm{NO_2} \tag{R1}$$

$$\mathrm{NO_2} \xrightarrow{h\nu} \mathrm{NO}. \tag{R2}$$

As NO_x is in steady state for the daylight observations we isolate, NO_2 can be calculated as follows:

$$\mathrm{NO_2} = \mathrm{NO} \times \left(\frac{k_1\,[\mathrm{O_3}] + k_2\,[\mathrm{HO_2}] + k_3\,[\mathrm{BrO}]}{j_{\mathrm{NO_2}}} \right). \tag{1}$$

Compounds in square brackets are in molecules cm^{-3}. NO and NO_2 are in pptv. Terms not introduced yet include the NO_2 photolysis frequency, j_{NO_2}, in s^{-1}; bromine monoxide (BrO); and rate constants of NO oxidation (Reaction R1) (k_{1-3}) in cm^3 molecule^{-1} s^{-1}. Temperature-dependent values of k_{1-3} are those recommended by the Jet Propulsion Laboratory (JPL) (Burkholder et al., 2020), calculated using DC-8 ambient temperature measurements. NO, $[O_3]$, and j_{NO_2} are from the DC-8 measurements, and $[HO_2]$ is from the DC-8 measurements for all campaigns except SEAC^{4}RS when it was not measured. We use GEOS-Chem (detailed in Sect. 2.3) simulated $[HO_2]$ to estimate SEAC^{4}RS PSS NO_2. [BrO] is obtained from GEOS-Chem for all campaigns. NO is also converted to NO_2 by organic peroxy radicals (RO_2), but we ignore this reaction as it is relatively insignificant throughout the free troposphere (Shah et al., 2023).

The NO_y components not measured during specific campaigns are inferred. These include HNO_4 for KORUS-AQ and ATom-3-4, PPN for ATom-1-2, and MPN for ARCTAS, ATom-1-4, and KORUS-AQ. The approaches used to infer these values differ, informed by the results; therefore, a detailed description of this inference is provided in Sect. 3.2.

2.2 Commercial aircraft observations of total NO_y

We use routine observations of upper tropospheric total NO_y from instruments on commercial long-haul passenger aircraft to determine if the intermittency and brevity of DC-8 campaign observations are representative of climatological conditions. The In-service Aircraft for a Global Observing System (IAGOS) European research infrastructure (Boulanger et al., 2018) provides routine in situ measurements of NO_y (Petzold et al., 2015). These are available from two IAGOS programmes: the Measurement of Ozone and Water Vapor by Airbus In-Service Aircraft (MOZAIC) (Marenco et al., 1998) from 2001 to 2005 (Volz-Thomas et al., 2005) and the Civil Aircraft for the Regular Investigation of the Atmosphere Based on an Instrument Container (CARIBIC) since December 2004 (Brenninkmeijer et al., 2007; Stratmann et al., 2016).

We consider the MOZAIC and CARIBIC observations together (collectively named IAGOS), as both programmes employed a chemiluminescence instrument with the same NO_y detection technique (Volz-Thomas et al., 2005; Brenninkmeijer et al., 2007). Direct intercomparison of NO_y is not possible, as there is no overlap in MOZAIC and CARIBIC NO_y. Data from 2003 to 2019 are used: 2003–2005 for MOZAIC and 2005–2019 for CARIBIC. We isolate daytime, upper tropospheric observations by applying the same O_3 tropopause, stratospheric O_3 intrusion, and daytime filtering as is applied to DC-8 data (Sect. 2.1), using IAGOS O_3 and CO measurements. There are no NO_2 photolysis frequency measurements, but the requirement for spatial coincidence with ATom excludes polar twilight and night measurements at high latitudes. We do not screen for observations impacted by fresh emissions, vertical convection, or biomass burning plumes, due to unavailability of concurrent measurements of suitable chemical tracers in the IAGOS data. As we consider 17 years of IAGOS data, we assume that the influence of these is dampened in the long-term median of NO_y. Both the IAGOS and DC-8 data are gridded to the same 2° latitude × 2.5° longitude grid.

2.3 The GEOS-Chem model

We use the GEOS-Chem global 3D chemical transport model version 13.0.2 (https://doi.org/10.5281/zenodo.4681204, The International GEOS-Chem User Community, 2021) to represent contemporary understanding of upper tropospheric NO_y for comparison to DC-8. The model is driven with consistent MERRA-2 assimilated meteorology at $2^\circ \times 2.5^\circ$ (latitude × longitude) over 47 vertical layers from the surface of the Earth to 0.01 hPa. The model emissions local to the upper troposphere include cruising altitude aircraft from the Aviation Emissions Inventory Code (AEIC) (Stettler et al., 2011) and lightning emissions as described in Murray et al. (2012). Surface emissions of NO_x and VOC precursors of ALKNs and PNs are from the anthropogenic Community Emissions Data System (CEDS) inventory of Hoesly et al. (2018); the Model of Emissions of Gases and Aerosols from Nature (MEGAN) biogenic VOC inventory version 2.1 (Guenther et al., 2012); the soil NO_x emission inventory of Hudman et al. (2012); and the Global Fire Emissions Database version 4 with small fires (GFED4s) for open burning of biomass (Giglio et al., 2013). Wet deposition of gas-phase HNO_3, the terminal sink for NO_y subsiding from the upper troposphere, includes in-cloud (rainout) and below-cloud (washout) scavenging as detailed in Amos et al. (2012) and enhanced scavenging as described by Luo et al. (2020).

We sample the model at the same time and location as the DC-8 observations using the ObsPack diagnostic (https://www.esrl.noaa.gov/gmd/ccgg/obspack/, last access: 23 October 2021), following a minimum 10-month spin-up preceding each campaign to initialize chemistry and large-scale circulation throughout the troposphere. Modelled components of NO_y include NO, NO_2, HNO_3, HNO_4, PAN, PPN, peroxymethacroyl nitrate (MPAN), MPN, and ALKNs.

3 Results and discussion

3.1 DC-8 campaign NO_y seasonality and budget closure

Figure 3 compares seasonality in UT NO_y from IAGOS and DC-8. Most of the overlap is with ATom along the North Atlantic flight corridor in all seasons, ARCTAS over the Canadian Arctic and Greenland in March–May (MAM) and June–August (JJA), and $SEAC^4RS$ over the Southeast US in September–November (SON). IAGOS NO_y exhibits similar peaks in spring (563 pptv) and summer (565 pptv), due to intensive seasonal lightning in the Northern Hemisphere (Stratmann et al., 2016). The decline in this source decreases NO_y in autumn to 365 pptv, and NO_y further decreases in winter to an annual minimum of 284 pptv.

DC-8 NO_y seasonality is similar to that of IAGOS, though the magnitude of DC-8 NO_y is consistently, on average, $\sim$ 130 pptv (range of 80 pptv in SON to 170 pptv in DJF) less than IAGOS NO_y in all seasons. The $\sim$ 130 pptv greater IAGOS NO_y likely results from differences in sampling altitudes. The two campaigns sample distinct altitude ranges of the upper portion of the upper troposphere centred at $\sim$ 240 hPa ($\sim$ 10 km) for IAGOS and a wider vertical extent of the lower portion of the upper troposphere centred at $\sim$ 360 hPa ($\sim$ 1.5 km below IAGOS) for DC-8 (Fig. S1 in the Supplement). There is a general pattern of a steep increase in NO_y with altitude, with the exception of IAGOS layers located near 300 hPa in March–May and September–November (Fig. S1). Average NO_y is similar between the two campaigns for the rare instances that DC-8 and IAGOS sample the same pressure layers (Fig. S1). Another minor factor may be IAGOS NO_y instrument interference from HCN. The IAGOS chemiluminescence instruments use a hydrogen (H_2) reagent to convert oxygenated nitrogen compounds to NO, whereas DC-8 uses CO, a compound not permitted on commercial aircraft (Bradshaw et al., 1998; Volz-Thomas et al., 2005; Thomas et al., 2015). The H_2 reagent

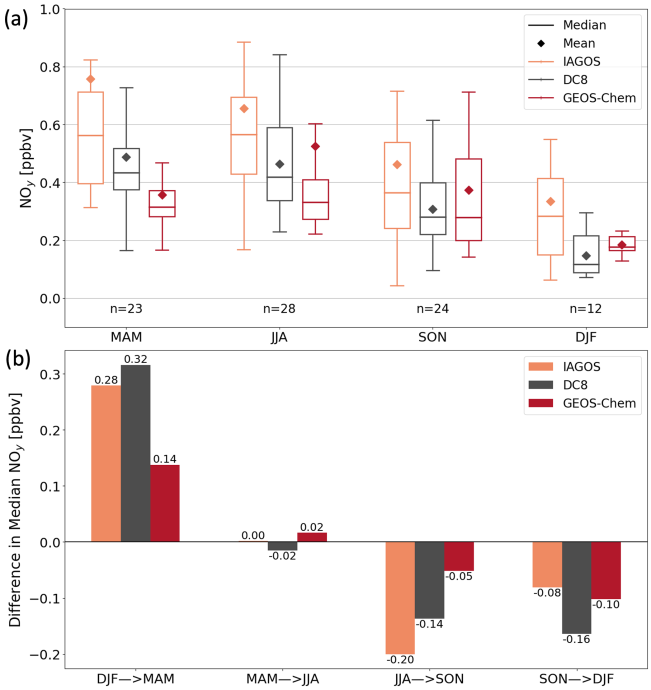

Figure 3. Seasonality of Northern Hemisphere upper tropospheric NO$_y$. Panels show seasonal means and medians **(a)** and seasonal transitions **(b)** of collocated gridded 2° × 2.5° NO$_y$ from IAGOS (orange), DC-8 (grey), and GEOS-Chem (red). Data in **(a)** are medians (lines), 25th and 75th percentiles (boxes), and means (diamonds). Inset text in **(a)** gives the number (n) of overlapping grid cells. Seasonality in **(b)** is the change in median NO$_y$ in **(a)** from one season to the next.

converts anywhere from 2 % to 20 % of HCN to NO$_y$ (Weinheimer, 2006). HCN ambient concentrations typically seasonally vary from ∼200 to 300 pptv in the upper troposphere, amounting to an interference of 4–60 pptv (Li et al., 2003; Le Breton et al., 2013).

Figure 4 shows the relationship between the sum of individual NO$_y$ components and total NO$_y$ for each DC-8 campaign. We use these scatterplots to determine whether most NO$_y$ components are measured in each campaign, given our intention to use DC-8 to assess contemporary understanding of upper tropospheric NO$_y$. The instruments and individual components of NO$_y$ summed for comparison with total NO$_y$ are listed in Table 1. The measured components include NO; PSS NO$_2$ (Eq. 1); HNO$_3$; PAN measured as PAN for all ATom sub-campaigns and as part of total PNs for ARCTAS, SEAC^{4}RS, and KORUS-AQ; HNO$_4$ measured as HNO$_4$ for ATom-1 and -2 and as part of total PNs for ARCTAS, SEAC^{4}RS, and KORUS-AQ; C1–C5 ALKNs for all ATom sub-campaigns; total ALKNs for SEAC^{4}RS, KORUS-AQ, and ARCTAS; PPN and other PANs for all except ATom-1 and -2; and MPN as part of total PNs for ARCTAS, SEAC^{4}RS, and KORUS-AQ. The evaluation in Fig. 4 is biased towards the Northern Hemisphere, as the low time resolution sampling of the WAS C1–C5 ALKNs during ATom leads to loss of data in the Southern Hemisphere (Fig. 2) to achieve coincidence of DC-8 total and individual components of NO$_y$.

Total measured NO$_y$ and the sum of individual NO$_y$ components are strongly correlated ($r > 0.8$) for all campaigns except SEAC^{4}RS ($r = 0.66$). The weaker correlation for SEAC^{4}RS is due to the large contribution of MPN to total PNs measured by the TD-LIF instrument, leading to a large contribution of MPN to total NO$_y$ for many of the points that stray most from the 1 : 1 line (Fig. S2). If instead we replace TD-LIF PNs with the sum of CIMS PANs and HNO$_4$, the correlation with total measured NO$_y$ increases to $r = 0.91$, but the regression slope decreases from 0.97 in Fig. 4 to 0.82, as MPN is ∼20 % of SEAC^{4}RS NO$_y$. The large contribution of MPN to total NO$_y$ during SEAC^{4}RS (Fig. S2) results from aged air initially influenced by lightning, biomass burning, and deep convective uplift of surface pollution with large quantities of VOCs and NO$_x$. These large quantities of VOCs and NO$_x$ cause very active photochemistry that enhances the abundance of the MPN precursor, CH$_3$O$_2$ (Browne et al., 2011; Nault et al., 2015).

The regression slopes in Fig. 4 indicate that most NO$_y$ components are measured during each campaign, ranging from 0.78 for ATom-2 (78 % of individual NO$_y$ components measured) to 0.99 for ATom-4 (99 % measured). The slopes suggest that between 1 % and 22 % of NO$_y$ originates from factors such as unmeasured components, positive interference in the NO$_y$ instrument, or a low bias in the TD-LIF PNs. Bradshaw et al. (1998) estimated a temperature-dependent interference from HCN of 8 %–15 % for chemiluminescence instruments that, like those deployed on DC-8 campaigns, use a CO reagent. We estimate a lower-end (8 %) interference for mean ambient upper troposphere temperatures measured along the flight paths in Fig. 2. Using DC-8 HCN observations, this amounts to ∼53 ppt or 12 % of NO$_y$ for ARCTAS, ∼19 pptv or 5 % of NO$_y$ for SEAC^{4}RS, ∼40 pptv or 6 % of NO$_y$ for KORUS-AQ, and ∼17 pptv or 6 % of NO$_y$ for ATom 1-4. These lower-end interference estimates are similar in size to the percent of unaccounted NO$_y$ (13 % for ARCTAS, 3 % for SEAC^{4}RS, 8 % for KORUS-AQ, 1 %–22 % for ATom).

Chemiluminescence NO$_y$ instruments also measure pNO$_3$ but with uncertain sampling efficiencies (Bourgeois et al., 2022). For 100 % sampling efficiency, we use the aerosol mass spectrometer (AMS) measurements of submicron (< 1 µm) pNO$_3$ to estimate a pNO$_3$ contribution that is at most 1 % of NO$_y$ for ARCTAS for a median pNO$_3$ of ∼0.01 µg m^{-3} (∼4 pptv), ∼4 % for SEAC^{4}RS for pNO$_3$ of ∼0.04 µg m^{-3} (∼14 pptv), ∼4 % for KORUS-AQ for pNO$_3$ ∼0.07 µg m^{-3} (∼25 pptv), and < 2 % for ATom for pNO$_3$ < 0.01 µg m^{-3} (∼4 pptv).

TD-LIF measurements of PNs are calculated from the difference in NO$_2$ detected with the NO$_2$ channel and with the PNs channel set to a temperature at which all PNs decompose

Table 1. Observations of individual NO_y components summed to assess budget closure in Fig. 4.

Component	NASA DC-8 aircraft campaign		
	ARCTAS, SEAC^{4}RS, KORUS-AQ	ATom1-2	ATom3-4
NO_2	PSS	PSS	PSS
NO	Chemiluminescence (CL)	CL	CL
HNO_3	CIMS	CIMS	CIMS
HNO_4	TD-LIF PNs	CIMS	–
PAN	TD-LIF PNs	PANTHER	PANTHER
PPN	TD-LIF PNs	–	CIMS
other PANs	TD-LIF PNs	–	CIMS
ALKNs	TD-LIF ALKNs	WAS C1–C5	WAS C1–C5
MPN	TD-LIF PNs	–	–

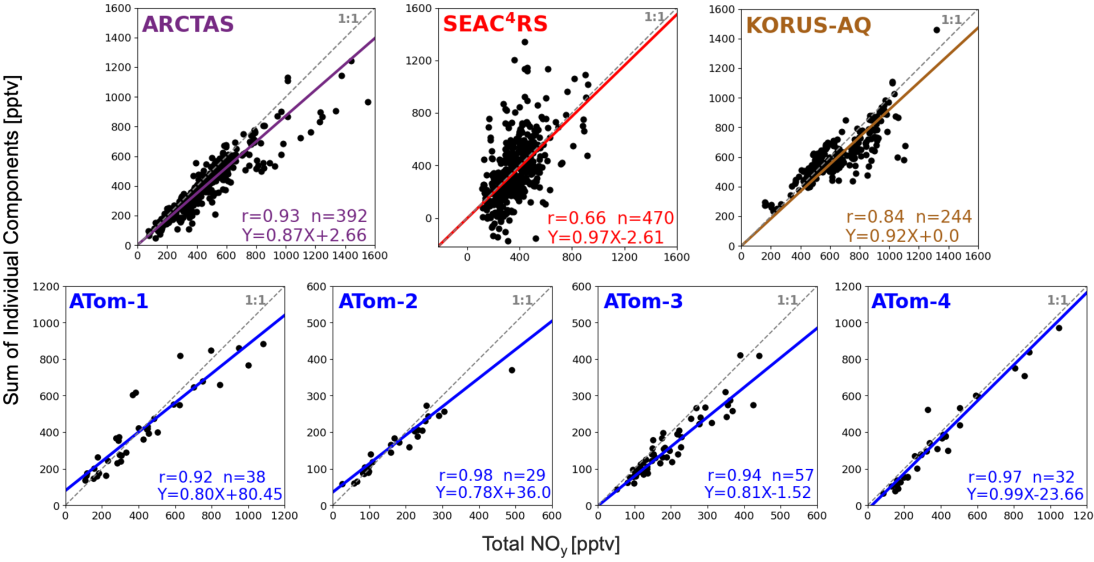

Figure 4. Proportion of reactive oxidized nitrogen components measured during each campaign. Individual points compare the coincident sum of individual NO_y components (Table 1) to measured total NO_y during NASA DC-8 campaigns. Individual NO_y components used in the figure are detailed in the text. Dashed grey lines represent the 1 : 1 relationship. Coloured lines and inset equations show the Theil–Sen regression fit to the observations. Other inset values are Pearson's correlation coefficients (r) and number of points (n). Axis ranges differ in each panel.

(Day et al., 2002). A bias in NO_2 could therefore impart a bias in PNs. The largest source of TD-LIF interference is the 100 % thermal decomposition of MPN (Reed et al., 2016b), and MPN during SEAC^{4}RS far exceeds that of any of the other campaigns. If we use the higher-end MPN interference of 21 % from Shah et al. (2023) for SEAC^{4}RS, this equates to ∼ 5 pptv of SEAC^{4}RS PSS NO_2. This is only ∼ 3 % of the 190 pptv SEAC^{4}RS PNs.

3.2 Upper tropospheric NO_y composition

Figure 5 provides a breakdown of the absolute and relative contributions of individual NO_y components to total NO_y. ATom-1 and -4 are combined, as these sub-campaigns have a very similar range in NO_y (Fig. 4) and in median total and individual components of NO_y, as the sampled seasons (spring and summer) have very similar NO_y (Fig. 3). Similarly, ATom-2 and -3 (autumn and winter) are combined. Campaigns are further grouped into remote (ARCTAS, ATom) and continental (SEAC^{4}RS, KORUS-AQ), as local influence from continental sources, like anthropogenic emissions and intense lightning, leads to a greater relative contribution of NO_x and lesser contribution of PAN for the continental upper troposphere and vice versa for the remote upper troposphere.

Inferred DC-8 HNO_4 and PPN in Fig. 5 use ATom-1 HNO_4 and ATom-4 PPN for combined ATom-1 and -4 components and, similarly, ATom-2 HNO_4 and ATom-3 PPN for combined ATom-2 and -3. KORUS-AQ HNO_4 is estimated to be 37 pptv by multiplying the SEAC^{4}RS median fraction of HNO_4 ($HNO_4/NO_y = 0.06$) by the KORUS-AQ median

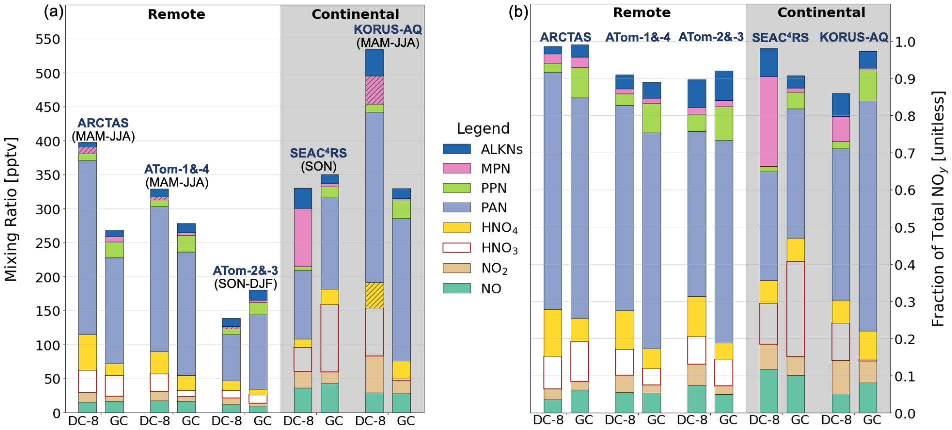

Figure 5. NO_y composition in the upper troposphere along DC-8 flight tracks. Bars represent the median values of absolute **(a)** and relative **(b)** individual NO_y components observed and inferred from observations during DC-8 campaigns and simulated by GEOS-Chem (GC). Seasons sampled are given above each bar **(a)**, and the grey shading distinguishes sampling in the remote (no shading) and continental (shaded) upper troposphere. Hatching in **(a)** indicates inferred concentrations (see text for details). Bar components from bottom to top are NO, NO_2, HNO_3, HNO_4, PAN, PPN, MPN, and ALKNs.

NO_y. SEAC^{4}RS is used because HNO_4 is thermally unstable (Ryerson et al., 2000) and so varies with temperature. Mean upper troposphere ambient temperatures for KORUS-AQ (252 K) are more consistent with SEAC^{4}RS (246 K) than the other campaigns (238 K for ARCTAS, 238–241 K for ATom).

The inferred ∼ 10 pptv ARCTAS MPN is from the estimate by Browne et al. (2011). KORUS-AQ MPN is estimated by bounding a potential range from two approaches. The first is the median value of the difference between TD-LIF total PNs and the sum of all individual CIMS PANs and our inferred HNO_4 of 37 pptv, yielding MPN = 75 pptv. This likely overestimates MPN, as the CIMS instrument does not measure an exhaustive suite of PANs. Lee et al. (2022) estimated with a box model and KORUS-AQ measurements that unmeasured PANs account for ∼ 20 % of total PNs during KORUS-AQ, though this applies to air masses impacted by petrochemical and other anthropogenic VOCs and NO_x emissions. Accounting for these unmeasured PANs yields a lower-bound KORUS-AQ MPN of 8 pptv. The MPN thus inferred for KORUS-AQ is 42 pptv, taken as the midpoint between 8 and 75 pptv, and it accounts for 7 % of KORUS-AQ NO_y. As the GEOS-Chem model MPN is consistent with DC-8 inferred MPN during ARCTAS, we multiply the GEOS-Chem ATom MPN fractions (MPN/NO_y ∼ 0.01 for ATom-1 and -4 and ∼ 0.02 for ATom-2 and -3) by ATom DC-8 NO_y to infer ATom MPN of < 6 pptv.

Only the C1–C5 ALKNs are shown in Fig. 5 for ATom. The remote measurements of total ALKNs available from ARCTAS that would be most suitable to assess the likely contribution of longer chain (> C5) ALKNs are on median 5 pptv less than the ATom C1–C5 ALKNs measurements. The ARCTAS total ALKNs measurements are also very noisy, as indicated by a range of −113 pptv to ∼ 333 pptv. The range in ARCTAS WAS C1–C5 measurements, by comparison, is 8–29 pptv. Contributions of > C5 ALKNs to total ALKNs for SEAC^{4}RS (∼ 50 %) and KORUS-AQ (∼ 60 %), representative of the continental upper troposphere, suggest that > C5 ALKNs in remote regions are < 50 % of total ALKNs or < 12 pptv (median of C1–C5 ALKNs for ATom1-4). According to the measurements, remote region C1–C5 ALKNs are dominated by methyl nitrate (C1 ALKN), accounting for 40 % of ATom C1–C5 ALKNs and 49 % for ARCTAS. Second is isopropyl nitrate (C3 ALKN), making up 17 % of ATom C1–C5 ALKNs and 25 % for ARCTAS. The > C3 ALKNs dominate ALKNs in the continental upper troposphere, accounting for 92 % of total ALKNs for SEAC^{4}RS and 71 % for KORUS-AQ. We estimate these as the difference between TD-LIF total ALKNs and the sum of WAS C1-C3 ALKNs.

The sum of KORUS-AQ NO_y components totals 531 pptv, > 130 pptv higher than SEAC^{4}RS, ARCTAS, and ATom-1 and -4, all of which are within a narrow range of 330–400 pptv. Minimum NO_y values are for the remote autumn and winter measurements from ATom-2 and -3 at 141 pptv. Despite the wide range in absolute total and components of NO_y, the relative contribution of many individual NO_y components is consistent across all campaigns. These include NO (7 ± 3 %; mean ± 1σ standard deviation), NO_2 (6 ± 2 %), HNO_3 (9 ± 2 %), HNO_4 (9 ± 3 %), PPN (3 ± 1 %), and ALKNs (5 ± 3 %). PAN, the dominant NO_y component in all campaigns, is least consistent, ranging from 30 %–41 % for the continental upper troposphere to 44 %–64 % for the remote upper troposphere. The HNO_4 fraction (10 %–13 %) in the remote upper troposphere is higher than in the continental upper troposphere (∼ 6 %), due to colder temperatures for ATom and ARCTAS. MPN is uniquely prominent during SEAC^{4}RS, accounting for 24 %

of NO_y compared to 2 %–7 % inferred for all other campaigns. pNO_3, absent in Fig. 5 due to the uncertain sampling efficiency of the chemiluminescence instrument, is at most 4 % for SEAC^{4}RS and KORUS-AQ (Sect. 3.1), comparable to the contribution from PPN.

The far larger fraction of MPN to total NO_y during SEAC^{4}RS (Fig. 5b) warrants further investigation, as the relative proportion of MPN to total NO_y ranges from negligible to 100 % (Fig. S2). If we instead estimate MPN by subtracting the sum of HNO_4 and all PANs measured with the CIMS instrument from the TD-LIF PNs, making the assumption that CIMS measures most PANs, MPN is 49 pptv and the SEAC^{4}RS median contribution to NO_y declines from 24 % to 14 %. This is still at least double the contribution for any other campaign. A small proportion of HNO_4 is measured in the MPN channel of the TD-LIF instrument. This represents about 11 %, according to Nault et al. (2015). For the CIMS median HNO_4 of 12.6 pptv during SEAC^{4}RS, the HNO_4 interference is only 1.4 pptv, so it does not affect the 14 %–24 % contribution.

The NO_y composition information in Fig. 5 has a Northern Hemisphere sampling bias to achieve coincidence. ATom observations south of the Equator exhibit a similar seasonal pattern to the Northern Hemisphere: summer > spring > autumn > winter NO_y, except that the Southern Hemisphere spring and summer NO_y differ by ∼ 90 pptv, whereas there is a near-negligible difference for the Northern Hemisphere (Fig. 3). As with the Northern Hemisphere, PAN accounts for most Southern Hemisphere NO_y, ranging from ∼ 32 % for ATom-1 (July–August) to ∼ 42 % for ATom-2 (January–February).

Nighttime-dominant NO_y compounds N_2O_5, NO_3, and HONO are not included in Fig. 5, as these have near-negligible daytime abundances. Of these, there are only measurements of N_2O_5, limited to ATom-3 and -4, that represent ∼ 0.1 % of upper tropospheric NO_y along the daytime ATom flight tracks in Fig. 2. NO_3 has a lifetime of a few seconds during the day, due to efficient photolysis (Brown and Stutz, 2012). HONO also rapidly photolyses with a near-surface lifetime of 15 min (Sörgel et al., 2011). Photolysis of HONO would be further enhanced (by ∼ 50 % at 390 nm) in the upper troposphere where photolysis frequencies are enhanced (Hofzumahaus et al., 2002; Reed et al., 2016a).

3.3 Contemporary understanding of UT NO_y

GEOS-Chem Northern Hemisphere upper troposphere NO_y is compared to the observations in Figs. 3 and 5. In Fig. 3, the GEOS-Chem median NO_y is less than that of DC-8 in summer and spring by ∼ 103 pptv, similar to that of DC-8 in autumn and greater than that of DC-8 in winter by ∼ 60 pptv. As a result of these differences in absolute NO_y, the model underestimates the IAGOS and DC-8 seasonal shifts in NO_y from winter to spring and from summer to autumn.

The sum of the GEOS-Chem fractional contributions of NO_y components in Fig. 5b does not equal 1 because the model NO_y budget also includes components not measured during DC-8 campaigns, such as MPAN and halogenated ALKNs. Consistent across all campaigns is a model underestimate of NO_2 and an overestimate of PPN. The model version we use does not include photolysis of PPN, even though this is known to occur (Harwood et al., 2003). PPN photolysis rather than thermal decomposition is the dominant loss pathway of PPN in the cold upper troposphere. PPN photolysis is scheduled for inclusion in a later model version (version 14.5) than that used here (Horner et al., 2024). Inclusion of PPN photolysis would liberate up to ∼ 16 pptv NO_2, resolving the 10–16 pptv model underestimate in NO_2. Other studies have addressed model biases in NO_2 by including photolysis of pNO_3 forming HONO that rapidly photolyses to NO_x (Shah et al., 2023; Horner et al., 2024). pNO_3 concentrations are too small in the upper troposphere for this to be a substantial NO_2 source. These are, on median, ∼ 0.01 $\mu g\,m^{-3}$ during ARCTAS, ∼ 0.07 $\mu g\,m^{-3}$ during KORUS-AQ, ∼ 0.04 $\mu g\,m^{-3}$ during SEAC^{4}RS, and < 0.01 $\mu g\,m^{-3}$ during ATom (Sect. 3.1).

The model exhibits significant campaign-specific biases in total NO_y for ARCTAS (129 pptv underestimate), KORUS-AQ (205 pptv underestimate), ATom-1 and -4 (51 pptv underestimate), and ATom-2 and -3 (42 pptv overestimate). The model underestimate in ARCTAS NO_y is due mostly to a ∼ 100 pptv low bias in PAN and, to a lesser extent, a 35 pptv underestimate in HNO_4. The model bias for ATom-2 and -3 is due almost entirely to PAN. For KORUS-AQ, all NO_y components except PPN are underestimated, indicative of an overall underestimate in NO_y sources to the upper troposphere over this region. The ATom-1 and -4 underestimation in NO_y is primarily due to a low model bias in PAN and HNO_3. Overall, the model underestimates the contrast in upper tropospheric NO_y between the remote and continental upper troposphere.

GEOS-Chem simulates individual C1-C3 ALKNs, but most > C3 ALKNs are included as a lumped species. There are other > C3 ALKNs represented individually in the model, such as those formed from isoprene oxidation (Fisher et al., 2016), but abundances of these are near negligible in the upper troposphere. DC-8 C1 ALKN is only 4 % of ALKNs for SEAC^{4}RS and 11 % for KORUS-AQ, whereas in the model these are a much greater component of ALKNs: 40 % for SEAC^{4}RS and 29 % for KORUS-AQ. Modelled > C3 ALKNs are a far smaller portion of total ALKNs (29 % for SEAC^{4}RS and 23 % for KORUS-AQ) than the observations (Sect. 3.2). Modelled C1 ALKN concentrations are consistently less than the observed values by ∼ 2 pptv for ARCTAS and ∼ 1 pptv for ATom. Modelled C3 ALKN is ∼ 1 pptv lower than the observations for ARCTAS but ∼ 1 pptv higher than the observations for ATom.

The sum of measured and modelled individual NO_y components is not significantly different for SEAC^{4}RS, though the model overestimates HNO_3 by 64 pptv and underestimates MPN by 81 pptv compared to the TD-LIF measurements and by 45 pptv compared to MPN inferred using TD-LIF PNs and CIMS measurements of HNO_4 and PANs (Sect. 3.2). The low bias in the model in MPN suggests that the model underestimates the influence of NO_x and reactive VOC sources on aged air over source regions with a mix of emissions from fires and lightning and deep convective injection of surface pollution. Chen et al. (2019) estimated that the GEOS-Chem underestimate in free-tropospheric VOCs during SEAC^{4}RS is on average ∼ 60 % but exceeds a factor of 2 for many of the VOCs assessed. The high bias in modelled HNO_3 during SEAC^{4}RS (Fig. 5) could be because of a factor of 2 overestimate in modelled H_2O_2 compared to observed H_2O_2 for SEAC^{4}RS. An overestimate in H_2O_2 indicates a model overestimate in HO_2 that promotes formation of HNO_3 and that would also account for the ∼ 10 pptv overestimate in modelled HNO_4. Modelled HO_2 is used to calculate PSS NO_2 for SEAC^{4}RS (Eq. (1), Sect. 2.1), but this only imparts a small high bias (∼ 1.7 pptv) in SEAC^{4}RS PSS NO_2. Model bias in H_2O_2 for ARCTAS (> 100 pptv) may also be responsible for the model underestimate in ARCTAS HNO_4 of ∼ 35 pptv.

Modelled KORUS-AQ HNO_3, ALKNs, and MPN are all biased low. The low biases in these NO_y components may be because of a general underestimate in NO_y sources over South Korea where there are large anthropogenic NO_x and VOC sources that are represented in the model with a global inventory (CEDS) that may not suitably account for local emissions (Travis et al., 2024). Lightning NO_x emissions could also be underestimated in the heavily parameterized inventory in GEOS-Chem (Murray et al., 2012; Marais et al., 2018), but this is a challenging NO_x source to evaluate over locations that include other prominent sources of NO_x.

The model biases identified in this work hinder the accurate determination of the radiative effect of tropospheric ozone for short-term climate impact assessments, the oxidative capacity of the troposphere in quantifying the lifetime and persistence of the greenhouse gas methane, tropospheric column densities of NO_2 from space-based UV-visible instruments that are retrieved with modelled vertical profiles of NO_2, NO_x emissions by means of comparing modelled and observed oxidized nitrate wet deposition fluxes that depend on the abundance of soluble HNO_3, and harm from nitrogen deposition to vulnerable habitats.

4 Conclusions

We used NASA DC-8 aircraft measurement data from the ARCTAS, SEAC^{4}RS, KORUS-AQ, and ATom campaigns to characterize reactive oxidized nitrogen (NO_y) in the global upper troposphere. This followed confirmation from comparison to routine total NO_y measurements from the IAGOS commercial aircraft campaign that DC-8 has the same seasonality as peak NO_y in summer and spring and minimum NO_y in winter in the Northern Hemisphere. Consistency supports the use of DC-8 campaign data to characterize NO_y under standard daytime conditions.

We also confirm that most (78 %–99 %) NO_y components were measured during DC-8 campaigns. These include nitrogen oxides (NO_x) and inorganic (HNO_3 and HNO_4) and organic (PANs, MPN, and alkyl nitrates) reservoirs of NO_x. PAN is the dominant NO_y component for all campaigns (30 %–64 %), followed by NO_x (6 %–18 %), HNO_4 (6 %–13 %), and HNO_3 (7 %–11 %). The relative contribution of most other components is similar across all campaigns, except for MPN. MPN is 14 %–24 % of NO_y for SEAC^{4}RS over the Southeast US and much less (2 %–7 %) for all other campaigns, though MPN measurements are rare and susceptible to biases.

The GEOS-Chem model is sampled along the DC-8 flight tracks to assess the state of knowledge of upper tropospheric NO_y. Consistent model biases for all campaigns include an overestimate in PPN and underestimate in NO_2. The model lacks PPN photolysis that would address the PPN model bias and mostly resolve the NO_2 bias. In the continental upper troposphere, the model underestimates total NO_y for KORUS-AQ but reproduces total NO_y for SEAC^{4}RS, though with too much HNO_3 and too little MPN. Over remote regions, the model biases are less severe and are likely related to the weak seasonal variability in total NO_y in comparison to DC-8 and IAGOS. A possible cause of this is errors in model representation of maritime lightning NO_x emissions that influence NO_y abundance in spring and summer.

Our results underscore the need for sustained measurements of upper tropospheric reactive oxidized nitrogen for further refinement of knowledge of upper tropospheric NO_y sources, advection, and chemical processing. This is crucial for advancing our understanding of the global nitrogen cycle and its broader environmental impacts.

Code and data availability. All data and software used in this study are from publicly accessible repositories: Zenodo for GEOS-Chem (https://doi.org/10.5281/zenodo.4681204, The International GEOS-Chem User Community, 2021), the AERIS data service for IAGOS (Boulanger et al., 2018), and NASA data archives for ARCTAS (https://www-air.larc.nasa.gov/cgi-bin/ArcView/arctas?DC8=1, NASA, 2009), SEAC^{4}RS (https://www-air.larc.nasa.gov/cgi-bin/ArcView/seac4rs, NASA, 2015), KORUS-AQ (https://asdc.larc.nasa.gov/project/KORUS-AQ, NASA, 2017), and ATom (https://daac.ornl.gov/cgi-bin/dsviewer.pl?ds_id=1925, NASA, 2021).

Author contributions. The study concept was developed by EAM and NW. NW led the data analysis and simulated GEOS-Chem. The manuscript was initiated by NW and co-written by EAM. GL aided in data analysis, RGR in the use of ObsPack, and BS in the use of IAGOS NO_y observations. All authors reviewed and edited the manuscript.

Competing interests. The contact author has declared that none of the authors has any competing interests.

Acknowledgements. We are grateful for the provision of the NASA DC-8 aircraft observations by the instrument PIs Paul O. Wennberg, Ronald C. Cohen, Thomas B. Ryerson, Chelsea Thompson, Andrew Weinheimer, L. Gregory Huey, Jim Elkins, and Donald R. Blake, as well as for the IAGOS-Core data provided by Andreas Volz-Thomas and IAGOS-CARIBIC data by Helmut Ziereis. The authors acknowledge the strong support of the European Commission, Airbus, and the airlines (Lufthansa, Air France, Austrian Airlines, Air Namibia, Cathay Pacific, Iberia, and China Airlines to date) for carrying the IAGOS-Core equipment and performing its maintenance since 1994. IAGOS-CARIBIC NO_y measurement funding was provided by the German Aerospace Centre (DLR). In its last 10 years of operation, IAGOS-Core has been funded by INSU–CNRS (France), Météo-France, Université Paul Sabatier (Toulouse, France), and Forschungszentrum Jülich (FZJ, Jülich, Germany). IAGOS has been additionally funded by the EU projects IAGOSDS and IAGOS-ERI. The IAGOS-Core and the IAGOS-CARIBIC databases are supported by AERIS. IAGOS-CARIBIC data are also available from the IAGOS-CARIBIC team (see http://www.caribic-atmospheric.com, last access: 23 May 2023).

Financial support. This research has been supported by the European Research Council under the European Union's Horizon 2020 research and innovation programme, through a Starting Grant awarded to Eloise A. Marais, UpTrop (grant no. 851854).

Review statement. This paper was edited by Benjamin A. Nault and reviewed by two anonymous referees.

References

Amos, H. M., Jacob, D. J., Holmes, C. D., Fisher, J. A., Wang, Q., Yantosca, R. M., Corbitt, E. S., Galarneau, E., Rutter, A. P., Gustin, M. S., Steffen, A., Schauer, J. J., Graydon, J. A., Louis, V. L. St., Talbot, R. W., Edgerton, E. S., Zhang, Y., and Sunderland, E. M.: Gas-particle partitioning of atmospheric Hg(II) and its effect on global mercury deposition, Atmos. Chem. Phys., 12, 591–603, https://doi.org/10.5194/acp-12-591-2012, 2012.

Barth, M. C., Cantrell, C. A., Brune, W. H., Rutledge, S. A., Crawford, J. H., Huntrieser, H., Carey, L. D., MacGorman, D., Weisman, M., Pickering, K. E., Bruning, E., Anderson, B., Apel, E., Biggerstaff, M., Campos, T., Campuzano-Jost, P., Cohen, R., Crounse, J., Day, D. A., Diskin, G., Flocke, F., Fried, A., Garland, C., Heikes, B., Honomichl, S., Hornbrook, R., Huey, L. G., Jimenez, J. L., Lang, T., Lichtenstern, M., Mikoviny, T., Nault, B., O'Sullivan, D., Pan, L. L., Peischl, J., Pollack, I., Richter, D., Riemer, D., Ryerson, T., Schlager, H., St. Clair, J., Walega, J., Weibring, P., Weinheimer, A., Wennberg, P., Wisthaler, A., Wooldridge, P. J., and Ziegler, C.: The Deep Convective Clouds and Chemistry (DC3) Field Campaign, B. Am. Meteorol. Soc., 96, 1281–1309, https://doi.org/10.1175/bams-d-13-00290.1, 2015.

Bertram, T. H., Perring, A. E., Wooldridge, P. J., Crounse, J. D., Kwan, A. J., Wennberg, P. O., Scheuer, E., Dibb, J., Avery, M., Sachse, G., Vay, S. A., Crawford, J. H., McNaughton, C. S., Clarke, A., Pickering, K. E., Fuelberg, H., Huey, G., Blake, D. R., Singh, H. B., Hall, S. R., Shetter, R. E., Fried, A., Heikes, B. G., and Cohen, R. C.: Direct measurements of the convective recycling of the upper troposphere, Science, 315, 816–820, https://doi.org/10.1126/science.1134548, 2007.

Blake, N. J., Blake, D. R., Swanson, A. L., Atlas, E., Flocke, F., and Rowland, F. S.: Latitudinal, vertical, and seasonal variations of C1-C4 alkyl nitrates in the troposphere over the Pacific Ocean during PEM-Tropics A and B: Oceanic and continental sources, J. Geophys. Res.-Atmos., 108, 8242, https://doi.org/10.1029/2001JD001444, 2003.

Blakeslee, R. J., Mach, D. M., Bateman, M. G., and Bailey, J. C.: Seasonal variations in the lightning diurnal cycle and implications for the global electric circuit, Atmos. Res., 135–136, 228–243, https://doi.org/10.1016/j.atmosres.2012.09.023, 2014.

Boersma, K. F., Eskes, H. J., Dirksen, R. J., van der A, R. J., Veefkind, J. P., Stammes, P., Huijnen, V., Kleipool, Q. L., Sneep, M., Claas, J., Leitão, J., Richter, A., Zhou, Y., and Brunner, D.: An improved tropospheric NO_2 column retrieval algorithm for the Ozone Monitoring Instrument, Atmos. Meas. Tech., 4, 1905–1928, https://doi.org/10.5194/amt-4-1905-2011, 2011.

Boulanger, D., Blot, R., Bundke, U., Gerbig, C., Hermann, M., Nédélec, P., Rohs, S., and Ziereis, H., IAGOS final quality controlled Observational Data L2 – Vertical profiles, AERIS [data set], https://doi.org/10.25326/07, 2018.

Bourgeois, I., Peischl, J., Neuman, J. A., Brown, S. S., Allen, H. M., Campuzano-Jost, P., Coggon, M. M., DiGangi, J. P., Diskin, G. S., Gilman, J. B., Gkatzelis, G. I., Guo, H., Halliday, H. A., Hanisco, T. F., Holmes, C. D., Huey, L. G., Jimenez, J. L., Lamplugh, A. D., Lee, Y. R., Lindaas, J., Moore, R. H., Nault, B. A., Nowak, J. B., Pagonis, D., Rickly, P. S., Robinson, M. A., Rollins, A. W., Selimovic, V., St. Clair, J. M., Tanner, D., Vasquez, K. T., Veres, P. R., Warneke, C., Wennberg, P. O., Washenfelder, R. A., Wiggins, E. B., Womack, C. C., Xu, L., Zarzana, K. J., and Ryerson, T. B.: Comparison of airborne measurements of NO, NO_2, HONO, NO_y, and CO during FIREX-AQ, Atmos. Meas. Tech., 15, 4901–4930, https://doi.org/10.5194/amt-15-4901-2022, 2022.

Bradshaw, J., Sandholm, S., and Talbot, R.: An update on reactive odd-nitrogen measurements made during recent NASA Global Tropospheric Experiment programs, J. Geophys. Res.-Atmos., 103, 19129–19148, https://doi.org/10.1029/98JD00621, 1998.

Bradshaw, J., Davis, D., Grodzinsky, G., Smyth, S., Newell, R., Sandholm, S., and Liu, S.: Observed distributions of nitrogen oxides in the remote free troposphere from the NASA Global Tropospheric Experiment Programs, Rev. Geophys., 38, 61–116, https://doi.org/10.1029/1999rg900015, 2000.

Brasseur, G. P., Müller, J.-F., and Granier, C.: Atmospheric impact of NO_x emissions by subsonic aircraft: A three dimensional model study, J. Geophys. Res.-Atmos., 101, 1423–1428, https://doi.org/10.1029/95jd02363, 1996.

Brenninkmeijer, C. A. M., Crutzen, P., Boumard, F., Dauer, T., Dix, B., Ebinghaus, R., Filippi, D., Fischer, H., Franke, H., Frieβ, U., Heintzenberg, J., Helleis, F., Hermann, M., Kock, H. H., Koeppel, C., Lelieveld, J., Leuenberger, M., Martinsson, B. G., Miemczyk, S., Moret, H. P., Nguyen, H. N., Nyfeler, P., Oram, D., O'Sullivan, D., Penkett, S., Platt, U., Pupek, M., Ramonet, M., Randa, B., Reichelt, M., Rhee, T. S., Rohwer, J., Rosenfeld, K., Scharffe, D., Schlager, H., Schumann, U., Slemr, F., Sprung, D., Stock, P., Thaler, R., Valentino, F., van Velthoven, P., Waibel, A., Wandel, A., Waschitschek, K., Wiedensohler, A., Xueref-Remy, I., Zahn, A., Zech, U., and Ziereis, H.: Civil Aircraft for the regular investigation of the atmosphere based on an instrumented container: The new CARIBIC system, Atmos. Chem. Phys., 7, 4953–4976, https://doi.org/10.5194/acp-7-4953-2007, 2007.

Brown, S. S. and Stutz, J.: Nighttime radical observations and chemistry, Chem. Soc. Rev., 41, 6405–6447, https://doi.org/10.1039/C2CS35181A, 2012.

Browne, E. C., Perring, A. E., Wooldridge, P. J., Apel, E., Hall, S. R., Huey, L. G., Mao, J., Spencer, K. M., Clair, J. M. St., Weinheimer, A. J., Wisthaler, A., and Cohen, R. C.: Global and regional effects of the photochemistry of CH3O2NO2: evidence from ARCTAS, Atmos. Chem. Phys., 11, 4209–4219, https://doi.org/10.5194/acp-11-4209-2011, 2011.

Burkholder, J. B., Sander, S. P., Abbatt, J., Barker, J. R., Cappa, C., Crounse, J. D., Dibble, T. S., Huie, R. E., Kolb, C. E., Kurylo, M. J., Orkin, V. L., Percival, C. J., Wilmouth, D. M., and Wine, P. H.: Chemical kinetics and photochemical data for use in atmospheric studies, evaluation No. 19, JPL Publication 19-5, https://jpldataeval.jpl.nasa.gov/pdf/NASA-JPL%20Evaluation%2019-5.pdf (last access: 20 May 2024), 2020.

Chen, X., Millet, D. B., Singh, H. B., Wisthaler, A., Apel, E. C., Atlas, E. L., Blake, D. R., Bourgeois, I., Brown, S. S., Crounse, J. D., de Gouw, J. A., Flocke, F. M., Fried, A., Heikes, B. G., Hornbrook, R. S., Mikoviny, T., Min, K.-E., Müller, M., Neuman, J. A., O'Sullivan, D. W., Peischl, J., Pfister, G. G., Richter, D., Roberts, J. M., Ryerson, T. B., Shertz, S. R., Thompson, C. R., Treadaway, V., Veres, P. R., Walega, J., Warneke, C., Washenfelder, R. A., Weibring, P., and Yuan, B.: On the sources and sinks of atmospheric VOCs: an integrated analysis of recent aircraft campaigns over North America, Atmos. Chem. Phys., 19, 9097–9123, https://doi.org/10.5194/acp-19-9097-2019, 2019.

Cohen, Y., Hauglustaine, D., Sauvage, B., Rohs, S., Konjari, P., Bundke, U., Petzold, A., Thouret, V., Zahn, A., and Ziereis, H.: Evaluation of modelled climatologies of O_3, CO, water vapour and NOy in the upper troposphere–lower stratosphere using regular in situ observations by passenger aircraft, Atmos. Chem. Phys., 23, 14973–15009, https://doi.org/10.5194/acp-23-14973-2023, 2023.

Crawford, J. H., Ahn, J.-Y., Al-Saadi, J., Chang, L., Emmons, L. K., Kim, J., Lee, G., Park, J.-H., Park, R. J., Woo, J. H., Song, C.-K., Hong, J.-H., Hong, Y.-D., Lefer, B. L., Lee, M., Lee, T., Kim, S., Min, K.-E., Yum, S. S., Shin, H. J., Kim, Y.-W., Choi, J.-S., Park, J.-S., Szykman, J. J., Long, R. W., Jordan, C. E., Simpson, I. J., Fried, A., Dibb, J. E., Cho, S., and Kim, Y. P.: The Korea–United States Air Quality (KORUS-AQ) field study, Elementa, 9, 00163, https://doi.org/10.1525/elementa.2020.00163, 2021.

Crounse, J. D., McKinney, K. A., Kwan, A. J., and Wennberg, P. O.: Measurement of gas-phase yydroperoxides by Chemical Ionization Mass Spectrometry, Anal. Chem., 78, 6726–6732, https://doi.org/10.1021/ac0604235, 2006.

Culter, F.: NASA DC-8 Flying Laboratory Aircraft, https://ghrc.nsstc.nasa.gov/home/sites/default/files/cutler_dc8.pdf, (last access: 3 October 2024), 2009.

Dahlmann, K., Grewe, V., Ponater, M., and Matthes, S.: Quantifying the contributions of individual NO_x sources to the trend in ozone radiative forcing, Atmos. Environ., 45, 2860–2868, https://doi.org/10.1016/j.atmosenv.2011.02.071, 2011.

Dameris, M.: Stratosphere/Troposphere exchange and structure | Tropopause, in: Encyclopedia of Atmospheric Sciences, 2nd Edn., edited by: North, G. R., Pyle, J., and Zhang, F., Academic Press, Oxford, 269–272, https://doi.org/10.1016/B978-0-12-382225-3.00418-7, 2015.

Day, D. A., Wooldridge, P. J., Dillon, M. B., Thornton, J. A., and Cohen, R. C.: A thermal dissociation laser-induced fluorescence instrument for in situ detection of NO_2, peroxy nitrates, alkyl nitrates, and HNO_3, J. Geophys. Res.-Atmos., 107, 4046, https://doi.org/10.1029/2001jd000779, 2002.

Ehhalt, D. H., Rohrer, F., and Wahner, A.: Sources and distribution of NO_x in the upper troposphere at northern mid-latitudes, J. Geophys. Res.-Atmos., 97, 3725–3738, https://doi.org/10.1029/91JD03081, 1992.

Emmons, L. K., Carroll, M. A., Hauglustaine, D. A., Brasseur, G. P., Atherton, C., Penner, J., Sillman, S., Levy, H., Rohrer, F., Wauben, W. M. F., Van Velthoven, P. F. J., Wang, Y., Jacob, D., Bakwin, P., Dickerson, R., Doddridge, B., Gerbig, C., Honrath, R., Hübler, G., Jaffe, D., Kondo, Y., Munger, J. W., Torres, A., and Volz-Thomas, A.: Climatologies of NO_x and NO_y: A comparison of data and models, Atmos. Environ., 31, 1851–1904, https://doi.org/10.1016/s1352-2310(96)00334-2, 1997.

Fisher, J. A., Jacob, D. J., Travis, K. R., Kim, P. S., Marais, E. A., Chan Miller, C., Yu, K., Zhu, L., Yantosca, R. M., Sulprizio, M. P., Mao, J., Wennberg, P. O., Crounse, J. D., Teng, A. P., Nguyen, T. B., St. Clair, J. M., Cohen, R. C., Romer, P., Nault, B. A., Wooldridge, P. J., Jimenez, J. L., Campuzano-Jost, P., Day, D. A., Hu, W., Shepson, P. B., Xiong, F., Blake, D. R., Goldstein, A. H., Misztal, P. K., Hanisco, T. F., Wolfe, G. M., Ryerson, T. B., Wisthaler, A., and Mikoviny, T.: Organic nitrate chemistry and its implications for nitrogen budgets in an isoprene- and monoterpene-rich atmosphere: constraints from aircraft (SEAC4RS) and ground-based (SOAS) observations in the Southeast US, Atmos. Chem. Phys., 16, 5969–5991, https://doi.org/10.5194/acp-16-5969-2016, 2016.

Fisher, J. A., Atlas, E. L., Barletta, B., Meinardi, S., Blake, D. R., Thompson, C. R., Ryerson, T. B., Peischl, J., Tzompa-Sosa, Z. A., and Murray, L. T.: Methyl, ethyl, and propyl nitrates: Global distribution and impacts on reactive nitrogen in remote marine environments, J. Geophys. Res.-Atmos., 123, 12429–12451, https://doi.org/10.1029/2018jd029046, 2018.

Fuelberg, H. E., Hannan, J. R., van Velthoven, P. F. J., Browell, E. V., Bieberbach Jr., G., Knabb, R. D., Gregory, G. L., Pickering, K. E., and Selkirk, H. B.: A meteorological overview of the Subsonic Assessment Ozone and Nitrogen Oxide Experiment (SONEX) period, J. Geophys. Res.-Atmos., 105, 3633–3651, https://doi.org/10.1029/1999JD900917, 2000.

Giglio, L., Randerson, J. T., and van der Werf, G. R.: Analysis of daily, monthly, and annual burned area using the fourth-generation global fire emissions database (GFED4), J. Geophys. Res.-Biogeo., 118, 317–328, https://doi.org/10.1002/jgrg.20042, 2013.

Gressent, A., Sauvage, B., Defer, E., Pätz, H. W., Thomas, K., Holle, R., Cammas, J.-P., Nédélec, P., Boulanger, D., Thouret, V., and Volz-Thomas, A.: Lightning NO_x influence on large-scale NO_y and O_3 plumes observed over the northern mid-latitudes, Tellus B, 66, 25544, https://doi.org/10.3402/tellusb.v66.25544, 2014.

Gressent, A., Sauvage, B., Cariolle, D., Evans, M., Leriche, M., Mari, C., and Thouret, V.: Modeling lightning-NO_x chemistry on a sub-grid scale in a global chemical transport model, Atmos. Chem. Phys., 16, 5867–5889, https://doi.org/10.5194/acp-16-5867-2016, 2016.

Guenther, A. B., Jiang, X., Heald, C. L., Sakulyanontvittaya, T., Duhl, T., Emmons, L. K., and Wang, X.: The Model of Emissions of Gases and Aerosols from Nature version 2.1 (MEGAN2.1): an extended and updated framework for modeling biogenic emissions, Geosci. Model Dev., 5, 1471–1492, https://doi.org/10.5194/gmd-5-1471-2012, 2012.

Harwood, M. H., Roberts, J. M., Frost, G. J., Ravishankara, A. R., and Burkholder, J. B.: Photochemical Studies of $CH_3C(O)OONO_2$ (PAN) and $CH_3CH_2C(O)OONO_2$ (PPN): NO_3 Quantum Yields, J. Phys. Chem. A, 107, 1148–1154, https://doi.org/10.1021/jp0264230, 2003.

Hoesly, R. M., Smith, S. J., Feng, L., Klimont, Z., Janssens-Maenhout, G., Pitkanen, T., Seibert, J. J., Vu, L., Andres, R. J., Bolt, R. M., Bond, T. C., Dawidowski, L., Kholod, N., Kurokawa, J. I., Li, M., Liu, L., Lu, Z., Moura, M. C. P., O'Rourke, P. R., and Zhang, Q.: Historical (1750–2014) anthropogenic emissions of reactive gases and aerosols from the Community Emissions Data System (CEDS), Geosci. Model Dev., 11, 369–408, https://doi.org/10.5194/gmd-11-369-2018, 2018.

Hofzumahaus, A., Kraus, A., Kylling, A., and Zerefos, C. S.: Solar actinic radiation (280–420 nm) in the cloud–free troposphere between ground and 12 km altitude: Measurements and model results, J. Geophys. Res.-Atmos., 107, 8139, https://doi.org/10.1029/2001jd900142, 2002.

Horner, R. P., Marais, E. A., Wei, N., Ryan, R. G., and Shah, V.: Vertical profiles of global tropospheric nitrogen dioxide (NO_2) obtained by cloud slicing the TROPOspheric Monitoring Instrument (TROPOMI), Atmos. Chem. Phys., 24, 13047–13064, https://doi.org/10.5194/acp-24-13047-2024, 2024.

Hudman, R. C., Jacob, D. J., Turquety, S., Leibensperger, E. M., Murray, L. T., Wu, S., Gilliland, A. B., Avery, M., Bertram, T. H., Brune, W., Cohen, R. C., Dibb, J. E., Flocke, F. M., Fried, A., Holloway, J., Neuman, J. A., Orville, R., Perring, A., Ren, X., Sachse, G. W., Singh, H. B., Swanson, A., and Wooldridge, P. J.: Surface and lightning sources of nitrogen oxides over the United States: Magnitudes, chemical evolution, and outflow, J. Geophys. Res., 112, D12S05, https://doi.org/10.1029/2006jd007912, 2007.

Hudman, R. C., Moore, N. E., Mebust, A. K., Martin, R. V., Russell, A. R., Valin, L. C., and Cohen, R. C.: Steps towards a mechanistic model of global soil nitric oxide emissions: implementation and space based-constraints, Atmos. Chem. Phys., 12, 7779–7795, https://doi.org/10.5194/acp-12-7779-2012, 2012.

Huey, L. G.: Measurement of trace atmospheric species by chemical ionization mass spectrometry: Speciation of reactive nitrogen and future directions, Mass Spectrom. Rev., 26, 166–184, https://doi.org/10.1002/mas.20118, 2007.

Huntrieser, H., Lichtenstern, M., Scheibe, M., Aufmhoff, H., Schlager, H., Pucik, T., Minikin, A., Weinzierl, B., Heimerl, K., Pollack, I. B., Peischl, J., Ryerson, T. B., Weinheimer, A. J., Honomichl, S., Ridley, B. A., Biggerstaff, M. I., Betten, D. P., Hair, J. W., Butler, C. F., Schwartz, M. J., and Barth, M. C.: Injection of lightning-produced NO_x, water vapor, wildfire emissions, and stratospheric air to the UT/LS as observed from DC3 measurements, J. Geophys. Res.-Atmos., 121, 6638–6668, https://doi.org/10.1002/2015JD024273, 2016.

Jacob, D. J., Crawford, J. H., Maring, H., Clarke, A. D., Dibb, J. E., Emmons, L. K., Ferrare, R. A., Hostetler, C. A., Russell, P. B., Singh, H. B., Thompson, A. M., Shaw, G. E., McCauley, E., Pederson, J. R., and Fisher, J. A.: The Arctic Research of the Composition of the Troposphere from Aircraft and Satellites (ARCTAS) mission: design, execution, and first results, Atmos. Chem. Phys., 10, 5191–5212, https://doi.org/10.5194/acp-10-5191-2010, 2010.

Jaeglé, L., Jacob, D. J., Wang, Y., Weinheimer, A. J., Ridley, B. A., Campos, T. L., Sachse, G. W., and Hagen, D. E.: Sources and chemistry of NO_x in the upper troposphere over the United States, Geophys. Res. Lett., 25, 1705–1708, https://doi.org/10.1029/97gl03591, 1998.

Le Breton, M., Bacak, A., Muller, J. B. A., O'Shea, S. J., Xiao, P., Ashfold, M. N. R., Cooke, M. C., Batt, R., Shallcross, D. E., Oram, D. E., Forster, G., Bauguitte, S. J.-B., Palmer, P. I., Parrington, M., Lewis, A. C., Lee, J. D., and Percival, C. J.: Airborne hydrogen cyanide measurements using a chemical ionisation mass spectrometer for the plume identification of biomass burning forest fires, Atmos. Chem. Phys., 13, 9217–9232, https://doi.org/10.5194/acp-13-9217-2013, 2013.

Lee, Y. R., Huey, L. G., Tanner, D. J., Takeuchi, M., Qu, H., Liu, X., Ng, N. L., Crawford, J. H., Fried, A., Richter, D., Simpson, I. J., Blake, D. R., Blake, N. J., Meinardi, S., Kim, S., Diskin, G. S., Digangi, J. P., Choi, Y., Pusede, S. E., Wennberg, P. O., Kim, M. J., Crounse, J. D., Teng, A. P., Cohen, R. C., Romer, P. S., Brune, W., Wisthaler, A., Mikoviny, T., Jimenez, J. L., Campuzano-Jost, P., Nault, B. A., Weinheimer, A., Hall, S. R., and Ullmann, K.: An investigation of petrochemical emissions during KORUS-AQ: Ozone production, reactive nitrogen evolution, and aerosol production, Elementa, 10, 00079, https://doi.org/10.1525/elementa.2022.00079, 2022.

Levy II, H., Mahlman, J. D., and Moxim, W. J.: A stratospheric source of reactive nitrogen in the unpolluted troposphere, Geophys. Res. Lett., 7, 441–444, https://doi.org/10.1029/GL007i006p00441, 1980.

Levy II, H., Moxim, W. J., Klonecki, A. A., and Kasibhatla, P. S.: Simulated tropospheric NO_x: Its evaluation, global distribution and individual source contributions, J. Geophys Res.-Atmos., 104, 26279–26306, https://doi.org/10.1029/1999JD900442, 1999.

Li, Q., Jacob, D. J., Yantosca, R. M., Heald, C. L., Singh, H. B., Koike, M., Zhao, Y., Sachse, G. W., and Streets, D. G.: A global three-dimensional model analysis of the atmospheric budgets of HCN and CH_3CN: Constraints from aircraft and ground measurements, J. Geophys. Res.-Atmos., 108, 8827, https://doi.org/10.1029/2002JD003075, 2003.

Liang, Q., Rodriguez, J. M., Douglass, A. R., Crawford, J. H., Olson, J. R., Apel, E., Bian, H., Blake, D. R., Brune, W., Chin, M., Colarco, P. R., da Silva, A., Diskin, G. S., Duncan, B. N., Huey, L. G., Knapp, D. J., Montzka, D. D., Nielsen, J. E., Pawson, S., Riemer, D. D., Weinheimer, A. J., and Wisthaler, A.: Reactive nitrogen, ozone and ozone production in the Arctic troposphere and the impact of stratosphere-troposphere exchange, Atmos. Chem. Phys., 11, 13181–13199, https://doi.org/10.5194/acp-11-13181-2011, 2011.

Logan, J. A.: Nitrogen oxides in the troposphere: Global and regional budgets, J. Geophys. Res.-Oceans, 88, 10785–10807, https://doi.org/10.1029/JC088iC15p10785, 1983.

Luo, G., Yu, F., and Moch, J. M.: Further improvement of wet process treatments in GEOS-Chem v12.6.0: impact on global distributions of aerosols and aerosol precursors, Geosci. Model Dev., 13, 2879–2903, https://doi.org/10.5194/gmd-13-2879-2020, 2020.

Marais, E. A., Jacob, D. J., Choi, S., Joiner, J., Belmonte-Rivas, M., Cohen, R. C., Beirle, S., Murray, L. T., Schiferl, L. D., Shah, V., and Jaeglé, L.: Nitrogen oxides in the global upper troposphere: interpreting cloud-sliced NO_2 observations from the OMI satellite instrument, Atmos. Chem. Phys., 18, 17017–17027, https://doi.org/10.5194/acp-18-17017-2018, 2018.

Marais, E. A., Roberts, J. F., Ryan, R. G., Eskes, H., Boersma, K. F., Choi, S., Joiner, J., Abuhassan, N., Redondas, A., Grutter, M., Cede, A., Gomez, L., and Navarro-Comas, M.: New observations of NO_2 in the upper troposphere from TROPOMI, Atmos. Meas. Tech., 14, 2389–2408, https://doi.org/10.5194/amt-14-2389-2021, 2021.

Marenco, A., Thouret, V., Nédélec, P., Smit, H., Helten, M., Kley, D., Karcher, F., Simon, P., Law, K., Pyle, J., Poschmann, G., Von Wrede, R., Hume, C., and Cook, T.: Measurement of ozone and water vapor by Airbus in-service aircraft: The MOZAIC airborne program, an overview, J. Geophys. Res.-Atmos., 103, 25631–25642, https://doi.org/10.1029/98jd00977, 1998.

Mickley, L. J., Murti, P. P., Jacob, D. J., Logan, J. A., Koch, D. M., and Rind, D.: Radiative forcing from tropospheric ozone calculated with a unified chemistry-climate model, J. Geophys. Res.-Atmos., 104, 30153–30172, https://doi.org/10.1029/1999jd900439, 1999.

Murray, L. T., Jacob, D. J., Logan, J. A., Hudman, R. C., and Koshak, W. J.: Optimized regional and interannual variability of lightning in a global chemical transport model constrained by LIS/OTD satellite data, J. Geophys. Res.-Atmos., 117, D20307, https://doi.org/10.1029/2012jd017934, 2012.

Murray, L. T., Logan, J. A., and Jacob, D. J.: Interannual variability in tropical tropospheric ozone and OH: The role of lightning, J. Geophys. Res.-Atmos., 118, 11468–11480, https://doi.org/10.1002/jgrd.50857, 2013.

Murray, L. T., Fiore, A. M., Shindell, D. T., Naik, V., and Horowitz, L. W.: Large uncertainties in global hydroxyl projections tied to fate of reactive nitrogen and carbon, P. Natl. Acad. Sci. USA, 118, e2115204118, https://doi.org/10.1073/pnas.2115204118, 2021.

NASA: Airborne Science Data for Atmospheric Composition, NASA [data set], https://www-air.larc.nasa.gov/cgi-bin/ArcView/arctas?DC8=1, (last access: 24 October 2024), 2009.

NASA: Airborne Science Data for Atmospheric Composition, NASA [data set], https://www-air.larc.nasa.gov/cgi-bin/ArcView/seac4rs (last access: 24 October 2024), 2015.

NASA: EARTHDATA, Korea United States Air Quality Study, NASA [data set], https://asdc.larc.nasa.gov/project/KORUS-AQ (last access: 24 October 2024), 2017.

NASA: EARTHDATA, ATom: Merged Atmospheric Chemistry, Trace Gases, and Aerosols, Version 2, NASA [data set], https://daac.ornl.gov/cgi-bin/dsviewer.pl?ds_id=1925 (last access: 24 October 2024) , 2021.

Nault, B. A., Garland, C., Pusede, S. E., Wooldridge, P. J., Ullmann, K., Hall, S. R., and Cohen, R. C.: Measurements of $CH_3O_2NO_2$ in the upper troposphere, Atmos. Meas. Tech., 8, 987–997, https://doi.org/10.5194/amt-8-987-2015, 2015.

Petzold, A., Thouret, V., Gerbig, C., Zahn, A., Brenninkmeijer, C. A. M., Gallagher, M., Hermann, M., Pontaud, M., Ziereis, H., Boulanger, D., Marshall, J., Nédélec, P., Smit, H. G. J., Friess, U., Flaud, J.-M., Wahner, A., Cammas, J.-P., and Volz-Thomas, A.: Global-scale atmosphere monitoring by in-service aircraft – Current achievements and future prospects of the European Research Infrastructure IAGOS, Tellus B, 67, 28452, https://doi.org/10.3402/tellusb.v67.28452, 2015.

Pollack, I. B., Lerner, B. M., and Ryerson, T. B.: Evaluation of ultraviolet light-emitting diodes for detection of atmospheric NO_2 by photolysis - chemiluminescence, J. Atmos. Chem., 65, 111–125, https://doi.org/10.1007/s10874-011-9184-3, 2010.

Prather, M. J. and Jacob, D. J.: A persistent imbalance in HO_x and NO_x photochemistry of the upper troposphere driven by deep tropical convection, Geophys. Res. Lett., 24, 3189–3192, https://doi.org/10.1029/97GL03027, 1997.

Rap, A., Richards, N. A. D., Forster, P. M., Monks, S. A., Arnold, S. R., and Chipperfield, M. P.: Satellite constraint on the tropospheric ozone radiative effect, Geophys. Res. Lett., 42, 5074–5081, https://doi.org/10.1002/2015gl064037, 2015.

Reed, C., Brumby, C. A., Crilley, L. R., Kramer, L. J., Bloss, W. J., Seakins, P. W., Lee, J. D., and Carpenter, L. J.: HONO measurement by differential photolysis, Atmos. Meas. Tech., 9, 2483–2495, https://doi.org/10.5194/amt-9-2483-2016, 2016a.

Reed, C., Evans, M. J., Di Carlo, P., Lee, J. D., and Carpenter, L. J.: Interferences in photolytic NO2 measurements: explanation for an apparent missing oxidant?, Atmos. Chem. Phys., 16, 4707–4724, https://doi.org/10.5194/acp-16-4707-2016, 2016b.

Roberts, J. M.: The atmospheric chemistry of organic nitrates, Atmos. Environ. A-Gen., 24, 243–287, https://doi.org/10.1016/0960-1686(90)90108-Y, 1990.

Roberts, J. M., Williams, J., Baumann, K., Buhr, M. P., Goldan, P. D., Holloway, J., Hübler, G., Kuster, W. C., McKeen, S. A., Ryerson, T. B., Trainer, M., Williams, E. J., Fehsenfeld, F. C., Bertman, S. B., Nouaime, G., Seaver, C., Grodzinsky, G., Rodgers, M., and Young, V. L.: Measurements of PAN, PPN, and MPAN made during the 1994 and 1995 Nashville Intensives of the Southern Oxidant Study: Implications for regional ozone production from biogenic hydrocarbons, J. Geophys. Res.-Atmos., 103, 22473–22490, https://doi.org/10.1029/98JD01637, 1998.

Roberts, J. M., Flocke, F., Stroud, C. A., Hereid, D., Williams, E., Fehsenfeld, F., Brune, W., Martinez, M., and Harder, H.:

Ground-based measurements of peroxycarboxylic nitric anhydrides (PANs) during the 1999 Southern Oxidants Study Nashville Intensive, J. Geophys. Res.-Atmos., 107, ACH 1-1–ACH 1-10, https://doi.org/10.1029/2001JD000947, 2002.

Ryerson, T. B., Williams, E. J., and Fehsenfeld, F. C.: An efficient photolysis system for fast-response NO_2 measurements, J. Geophys. Res.-Atmos., 105, 26447–26461, https://doi.org/10.1029/2000JD900389, 2000.

Schultz, M. G., Jacob, D. J., Wang, Y., Logan, J. A., Atlas, E. L., Blake, D. R., Blake, N. J., Bradshaw, J. D., Browell, E. V., Fenn, M. A., Flocke, F., Gregory, G. L., Heikes, B. G., Sachse, G. W., Sandholm, S. T., Shetter, R. E., Singh, H. B., and Talbot, R. W.: On the origin of tropospheric ozone and NO_x over the tropical South Pacific, J. Geophys. Res.-Atmos., 104, 5829–5843, https://doi.org/10.1029/98jd02309, 1999.

Seltzer, K. M., Vizuete, W., and Henderson, B. H.: Evaluation of updated nitric acid chemistry on ozone precursors and radiative effects, Atmos. Chem. Phys., 15, 5973–5986, https://doi.org/10.5194/acp-15-5973-2015, 2015.

Shah, V., Jacob, D. J., Dang, R., Lamsal, L. N., Strode, S. A., Steenrod, S. D., Boersma, K. F., Eastham, S. D., Fritz, T. M., Thompson, C., Peischl, J., Bourgeois, I., Pollack, I. B., Nault, B. A., Cohen, R. C., Campuzano-Jost, P., Jimenez, J. L., Andersen, S. T., Carpenter, L. J., Sherwen, T., and Evans, M. J.: Nitrogen oxides in the free troposphere: implications for tropospheric oxidants and the interpretation of satellite NO2 measurements, Atmos. Chem. Phys., 23, 1227–1257, https://doi.org/10.5194/acp-23-1227-2023, 2023.

Silvern, R. F., Jacob, D. J., Travis, K. R., Sherwen, T., Evans, M. J., Cohen, R. C., Laughner, J. L., Hall, S. R., Ullmann, K., Crounse, J. D., Wennberg, P. O., Peischl, J., and Pollack, I. B.: Observed NO/NO_2 Ratios in the Upper Troposphere Imply Errors in NO-NO_2-O_3 Cycling Kinetics or an Unaccounted NO_x Reservoir, Geophys. Res. Lett., 45, 4466–4474, https://doi.org/10.1029/2018gl077728, 2018.

Singh, H. B.: Reactive nitrogen in the troposphere, Environ. Sci. Technol., 21, 320–327, https://doi.org/10.1021/es00158a001, 1987.

Singh, H. B., Thompson, A. M., and Schlager, H.: SONEX airborne mission and coordinated POLINAT-2 activity: Overview and accomplishments, Geophys. Res. Lett., 26, 3053–3056, https://doi.org/10.1029/1999GL900588, 1999.

Singh, H. B., Brune, W. H., Crawford, J. H., Jacob, D. J., and Russell, P. B.: Overview of the summer 2004 Intercontinental Chemical Transport Experiment–North America (INTEX-A), J. Geophys. Res.-Atmos., 111, D24S01, https://doi.org/10.1029/2006JD007905, 2006.

Singh, H. B., Brune, W. H., Crawford, J. H., Flocke, F., and Jacob, D. J.: Chemistry and transport of pollution over the Gulf of Mexico and the Pacific: spring 2006 INTEX-B campaign overview and first results, Atmos. Chem. Phys., 9, 2301–2318, https://doi.org/10.5194/acp-9-2301-2009, 2009.

Sörgel, M., Regelin, E., Bozem, H., Diesch, J.-M., Drewnick, F., Fischer, H., Harder, H., Held, A., Hosaynali-Beygi, Z., Martinez, M., and Zetzsch, C.: Quantification of the unknown HONO daytime source and its relation to NO_2, Atmos. Chem. Phys., 11, 10433–10447, https://doi.org/10.5194/acp-11-10433-2011, 2011.

Stettler, M. E. J., Eastham, S., and Barrett, S. R. H.: Air quality and public health impacts of UK airports. Part I: Emissions, Atmos. Environ., 45, 5415–5424, https://doi.org/10.1016/j.atmosenv.2011.07.012, 2011.

Stratmann, G., Ziereis, H., Stock, P., Brenninkmeijer, C. A. M., Zahn, A., Rauthe-Schöch, A., Velthoven, P. V., Schlager, H., and Volz-Thomas, A.: NO and NO_y in the upper troposphere: Nine years of CARIBIC measurements onboard a passenger aircraft, Atmos. Environ., 133, 93–111, https://doi.org/10.1016/j.atmosenv.2016.02.035, 2016.

Talbot, R. W., Dibb, J. E., Scheuer, E. M., Kondo, Y., Koike, M., Singh, H. B., Salas, L. B., Fukui, Y., Ballenthin, J. O., Meads, R. F., Miller, T. M., Hunton, D. E., Viggiano, A. A., Blake, D. R., Blake, N. J., Atlas, E., Flocke, F., Jacob, D. J., and Jaegle, L.: Reactive nitrogen budget during the NASA SONEX Mission, Geophys. Res. Lett., 26, 3057–3060, https://doi.org/10.1029/1999GL900589, 1999.

The International GEOS-Chem User Community: geoschem/GC-Classic: GEOS-Chem 13.0.2 (13.0.2), Zenodo [code], https://doi.org/10.5281/zenodo.4681204, 2021.

Thomas, K., Berg, M., Boulanger, D., Houben, N., Gressent, A., Nédélec, P., Pätz, H.-W., Thouret, V., and Volz-Thomas, A.: Climatology of NO_y in the troposphere and UT/LS from measurements made in MOZAIC, Tellus B, 67, 28793, https://doi.org/10.3402/tellusb.v67.28793, 2015.

Thompson, C. R., Wofsy, S. C., Prather, M. J., Newman, P. A., Hanisco, T. F., Ryerson, T. B., Fahey, D. W., Apel, E. C., Brock, C. A., Brune, W. H., Froyd, K., Katich, J. M., Nicely, J. M., Peischl, J., Ray, E., Veres, P. R., Wang, S., Allen, H. M., Asher, E., Bian, H., Blake, D., Bourgeois, I., Budney, J., Bui, T. P., Butler, A., Campuzano-Jost, P., Chang, C., Chin, M., Commane, R., Correa, G., Crounse, J. D., Daube, B., Dibb, J. E., Digangi, J. P., Diskin, G. S., Dollner, M., Elkins, J. W., Fiore, A. M., Flynn, C. M., Guo, H., Hall, S. R., Hannun, R. A., Hills, A., Hintsa, E. J., Hodzic, A., Hornbrook, R. S., Huey, L. G., Jimenez, J. L., Keeling, R. F., Kim, M. J., Kupc, A., Lacey, F., Lait, L. R., Lamarque, J.-F., Liu, J., Mckain, K., Meinardi, S., Miller, D. O., Montzka, S. A., Moore, F. L., Morgan, E. J., Murphy, D. M., Murray, L. T., Nault, B. A., Neuman, J. A., Nguyen, L., Gonzalez, Y., Rollins, A., Rosenlof, K., Sargent, M., Schill, G., Schwarz, J. P., St. Clair, J. M., Steenrod, S. D., Stephens, B. B., Strahan, S. E., Strode, S. A., Sweeney, C., Thames, A. B., Ullmann, K., Wagner, N., Weber, R., Weinzierl, B., Wennberg, P. O., Williamson, C. J., Wolfe, G. M., and Zeng, L.: The NASA Atmospheric Tomography (ATom) Mission: Imaging the chemistry of the global atmosphere, B. Am. Meteorol. Soc., 103, E761–E790, https://doi.org/10.1175/bams-d-20-0315.1, 2021.

Toon, O. B., Maring, H., Dibb, J., Ferrare, R., Jacob, D. J., Jensen, E. J., Luo, Z. J., Mace, G. G., Pan, L. L., Pfister, L., Rosenlof, K. H., Redemann, J., Reid, J. S., Singh, H. B., Thompson, A. M., Yokelson, R., Minnis, P., Chen, G., Jucks, K. W., and Pszenny, A.: Planning, implementation, and scientific goals of the Studies of Emissions and Atmospheric Composition, Clouds and Climate Coupling by Regional Surveys ($SEAC^4RS$) field mission, J. Geophys. Res.-Atmos., 121, 4967–5009, https://doi.org/10.1002/2015jd024297, 2016.

Travis, K. R., Jacob, D. J., Fisher, J. A., Kim, P. S., Marais, E. A., Zhu, L., Yu, K., Miller, C. C., Yantosca, R. M., Sulprizio, M. P., Thompson, A. M., Wennberg, P. O., Crounse, J. D., St. Clair,

J. M., Cohen, R. C., Laughner, J. L., Dibb, J. E., Hall, S. R., Ullmann, K., Wolfe, G. M., Pollack, I. B., Peischl, J., Neuman, J. A., and Zhou, X.: Why do models overestimate surface ozone in the Southeast United States?, Atmos. Chem. Phys., 16, 13561–13577, https://doi.org/10.5194/acp-16-13561-2016, 2016.

Travis, K. R., Heald, C. L., Allen, H. M., Apel, E. C., Arnold, S. R., Blake, D. R., Brune, W. H., Chen, X., Commane, R., Crounse, J. D., Daube, B. C., Diskin, G. S., Elkins, J. W., Evans, M. J., Hall, S. R., Hintsa, E. J., Hornbrook, R. S., Kasibhatla, P. S., Kim, M. J., Luo, G., McKain, K., Millet, D. B., Moore, F. L., Peischl, J., Ryerson, T. B., Sherwen, T., Thames, A. B., Ullmann, K., Wang, X., Wennberg, P. O., Wolfe, G. M., and Yu, F.: Constraining remote oxidation capacity with ATom observations, Atmos. Chem. Phys., 20, 7753–7781, https://doi.org/10.5194/acp-20-7753-2020, 2020.

Travis, K. R., Nault, B. A., Crawford, J. H., Bates, K. H., Blake, D. R., Cohen, R. C., Fried, A., Hall, S. R., Huey, L. G., Lee, Y. R., Meinardi, S., Min, K.-E., Simpson, I. J., and Ullman, K.: Impact of improved representation of volatile organic compound emissions and production of NO_x reservoirs on modeled urban ozone production, Atmos. Chem. Phys., 24, 9555–9572, https://doi.org/10.5194/acp-24-9555-2024, 2024.

Volz-Thomas, A., Berg, M., Heil, T., Houben, N., Lerner, A., Petrick, W., Raak, D., and Pätz, H.-W.: Measurements of total odd nitrogen (NO_y) aboard MOZAIC in-service aircraft: instrument design, operation and performance, Atmos. Chem. Phys., 5, 583–595, https://doi.org/10.5194/acp-5-583-2005, 2005.

Weinheimer, A. J.: Chemical Methods: Chemiluminscence, Chemical Amplification, Electrochemistry, and Derivation, in: Analytical Techniques for Atmospheric Measurement, 311–360, https://doi.org/10.1002/9780470988510.ch7, 2006.

Weinheimer, A. J., Walega, J. G., Ridley, B. A., Gary, B. L., Blake, D. R., Blake, N. J., Rowland, F. S., Sachse, G. W., Anderson, B. E., and Collins, J. E.: Meridional distributions of NO_x, NO_y, and other species in the lower stratosphere and upper troposphere during AASE II, Geophys. Res. Lett., 21, 2583–2586, https://doi.org/10.1029/94GL01897, 1994.

Worden, H. M., Bowman, K. W., Kulawik, S. S., and Aghedo, A. M.: Sensitivity of outgoing longwave radiative flux to the global vertical distribution of ozone characterized by instantaneous radiative kernels from Aura-TES, J. Geophys. Res., 116, D14115, https://doi.org/10.1029/2010jd015101, 2011.

Zahn, A., Brenninkmeijer, C. A. M., Asman, W. A. H., Crutzen, P. J., Heinrich, G., Fischer, H., Cuijpers, J. W. M., and van Velthoven, P. F. J.: Budgets of O_3 and CO in the upper troposphere: CARIBIC passenger aircraft results 1997–2001, J. Geophys. Res.-Atmos., 107, ACH 6-1–ACH 6-20, https://doi.org/10.1029/2001JD001529, 2002.